University of South-Eastern Norway

www.usn.no

FMH606 Master's Thesis 2020

MT-40-20

Simulation of Hydrogen Tank Refuelling

Masih Mojarrad

Faculty of Technology, Natural sciences and Maritime Sciences
Campus Porsgrunn

University of South-Eastern Norway

www.usn.no

Course: FMH606 Master's Thesis, 2020

Title: Simulation of hydrogen tank refuelling

Number of pages: 46

Keywords: CFD, Maximum temperature, Hydrogen, *k* and epsilon

Student: Masih Mojarrad

Supervisor: Prof. Knut Vågsæther

External partner: H_2 Maritime, Umoe Advanced Composites

Availability: Open

University of South-Eastern Norway

www.usn.no

Summary:

As an alternative to fossil fuels and as a sustainable energy carrier, there are considerable interests in investigating hydrogen. Hence, it seems significant to evaluate the behavior of hydrogen in refueling or storing. The most important issue in refueling the tank pertains to the temperature. The hydrogen inside the tank heats up during the filling due to the effect of compression and negative Joule-Thomson coefficient. As a result, the main aim of this project is to examine the temperature inside the tank to not exceed 85°C in order to avoid cracking in the wall and consequently, further possible disasters. This can be done by implementing simulation with a proper software.

OpenFoam is an appropriate software to consider such behaviors and it contributes to developing and considering the variety of properties including the temperature inside the tank. The cylindrical geometry is created with blockMesh in 3D while the geometry ends up with rectangular cubic in 2D. The proper boundary conditions and initial properties are set up in rhoCentralFoam solver to establish simulations in OpenFoam 5.0.

According to the obtained results, it is found out that it seems necessary to precool inlet hydrogen to fulfill the main purpose of this project. The bigger inlet area also decreases the maximum temperature inside the tank however this effect is not that much considerable compared to precooling. A further point to add is that the position of the inlet can play a significant role in the final temperature. Acquired results prove that the direction of inlet velocity should be aligned with the length of cylinder otherwise the temperature increases significantly.

At last, comparing the final results to what was calculated and expected reveals that the results have an acceptable concordance and consistency. So, it can be deduced that the simulations have been done properly and the results can be trusted for further studies or possible experiments.

Preface

This report presents the observation of the project “simulation of hydrogen tank refueling” established by OpenFoam. I would like to appreciate all my family, friends, and my teachers supporting me emotionally, technically, and financially these years in Norway. Also, I am really grateful for invaluable guidance and all contributes receiving from my supervisor, Prof. Knut Vågsæther.

Porsgrunn, May 10, 2020

Masih Mojarrad

Contents

1 Introduction 8

2 Theory of hydrogen tank refueling 9

2.1 Type of the tank 9
2.2 Initial Pressure 10
2.3 Inlet temperature 11
2.4 Heat transfer 11
2.5 Joule-Thomson effect 11

3 Theory of CFD 13

3.1 Transport Equation 13
3.2 Model of solving equations 14
3.3 Law of the wall 15
3.4 Finite Volume Method 16
3.5 Scheme 17
3.6 Boundary Types 18
3.7 Solver 18

4 Simulation Set-Up 19

4.1 Geometry and Size 19
4.2 Cases 21
4.3 Boundary Condition 21
4.3.1 Temperature 22
4.3.2 Pressure 22
4.3.3 K and epsilon 24
4.3.4 Velocity 24
4.4 fvSchemes 24
4.5 Thermodynamic Properties 25

5 Result and Comparison 27

5.1 3D vs 2D (Case I vs Case II) 27
5.2 Impact of changing the inlet diameter (Case II vs Case III) 29
5.3 Impact of inlet temperature (Case III vs Case IV) 31
5.4 Impact of changing the inlet position (Case III vs Case V) 33
5.5 Considering the temperature regulation 35
5.6 Validating the results 35

6 Conclusion 39

7 Further Study 41

Nomenclature

ρ	Fluid density [kg/m^3]
S_φ	Source term
φ	Fluid property
u	Fluid velocity in the x-direction
v	Fluid velocity in the y-direction
w	Fluid velocity in the z-direction
Γ	Diffusion coefficient [m^2/s]
ϑ	Kinematic viscosity [m^2/s]
τ	Shear stress [pa]
T_i	Turbulence intensity
L	characteristic length [m]
k	turbulent kinetic energy [m^2/s^2]
ε	turbulent dissipation [m^2/s^3]
Re	Reynolds number
Pe	Peclet number
h	heat transfer coefficient [W/m^{2}K]
v	relative speed [m/s]
μ	dynamic viscosity [Pa.s]
$\acute{D}$	self-diffusion [m^2/s]
P	pressure [bar]
V	volume [m^3]
M	molecular weight [kg/mole]
R	gas constant [J/mole.K]

m	mass [kg]
δx	cell width [m]
U	velocity [m/s]
C_p	heat capacity [J/K]
H	enthalpy [J]
S	entropy [J/K]
A_s	Sutherland coefficient [Pa.s/$\sqrt{K}$]
T_s	Sutherland temperature [K]

1 Introduction

During the last years, due to global warming, there has been considerable investment in hydrogen as a carbonless energy carrier. Nevertheless, based on safety, it seems important to consider international standards and regulations. For instance, as the process of filling a tank with hydrogen increases the temperature inside the tank due to compression and the Joule-Thomson effect, the temperature must not exceed 85°C according to the majority of standards like international standard ISO 15869. In other words, the rise of temperature causes the high rate of hydrogen embrittlement in the walls and that is why there is a maximum temperature being set [1-6].

There are many kinds of research regarding hydrogen refueling but, in this study, a rather big tank with a high rate of mass inlet flow is considered for the first time. This project can help to improve shipping applications in case of storing the hydrogen, transferring or using the storage tank as the source of the fuel as sustainable energy.

For investigating such topics, **C**omputational **F**luid **D**ynamic (CFD) analysis is fruitful. In most cases, the major concentration is on inlet temperature and initial pressure[1-4] however in this study, the inlet area and the position of the inlet have been also investigated. The initial pressure is 10 bar and the tank is filled with 200 kg hydrogen which leads the pressure inside the tank to reach about 250 bar.

In this report, the 3-dimensional and 2-dimensional tanks are simulated by OpenFoam 5.0. There, the inlet area, inlet temperature, and the position of the inlet are considered as variables while the inlet mass flow is constant being 1 kg/s. The upwind scheme seems suitable for this investigation due to the high rate of convection. Also, blockMesh is used for creating the geometry while rhoCentralFoam is the solver used for implementing the simulation.

2 Theory of hydrogen tank refueling

There are several parameters influencing the process which are necessary to consider like the temperature and the type of tank. These parameters are discussed in the following subchapters. Besides, a scheme of hydrogen tank is shown in Figure 2.1.

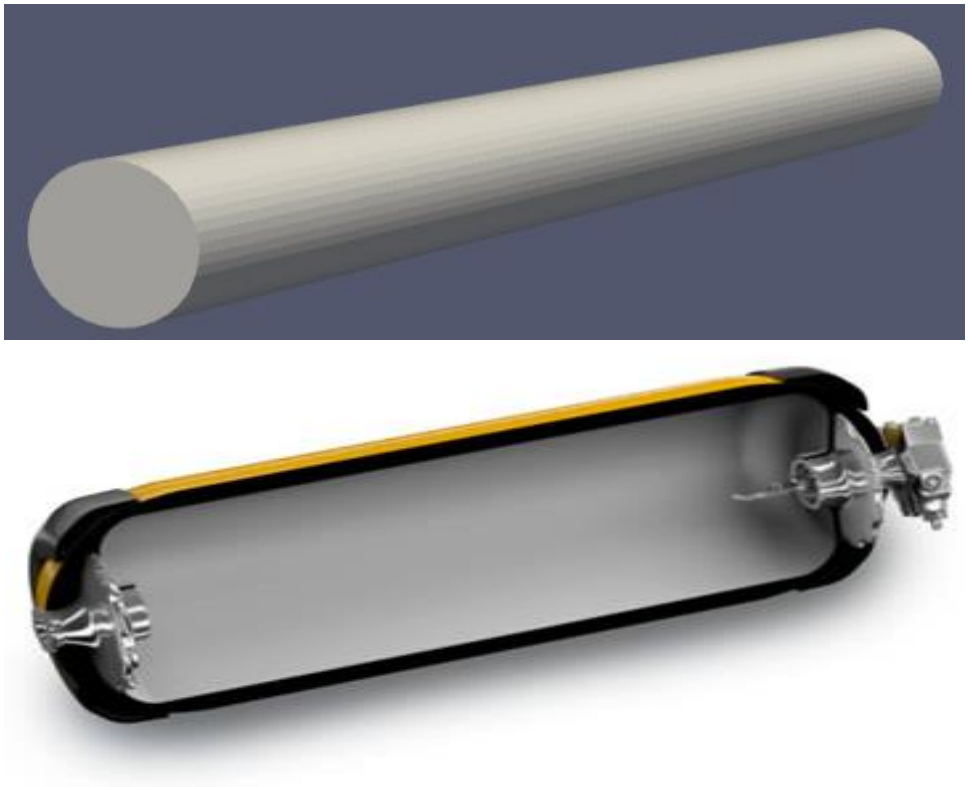

Figure 2.1: A scheme of hydrogen tank in reality[7] and in simulation.

2.1 Type of the tank

The material used for the hydrogen tank is another concern. There are four types of hydrogen tanks. Since refueling time plays a significant role in industrial application, type IV has the widest range of use which is made of carbon fiber reinforced plastic [4, 8]. The properties of different types of hydrogen tanks are listed in Table 2.1.

Table 2.1: Properties of different types of hydrogen tank [8]

Tank types	Materials	Features	Applications	Hydrogen storage pressure and mass percent (WT%)
Type I	All metal	Heavy, internal corrosion	For industrial, not suited for vehicular use	17.5-20 MPa 1 WT%
Type II	Metal liner with hoop wrapping	Heavy, short life due to internal corrosion	Not suited for vehicular use	26.3-30 MPa
Type III	Metal liner with full-composite wrapping	No permeation, galvanic corrosion between liner and fiber	Suited for vehicular use 25-75 % mass gain over I and II	35 MPa: 3.9 WT% -70MPa: 5 WT%
Type IV	Plastic liner with full-composite wrapping	Lightness, lower burst pressure Permeation through a liner, high durability against repeated changing Simple manufacturability	Longer life than Type III (no creep-fatigue)	70 MPa: more than 5 WT%

2.2 Initial Pressure

One of the significant factors to consider is initial pressure inside the tank. The higher the initial pressure, the lower the final temperature would be. In contrast, the higher initial pressure causes less hydrogen dispensing into the tank than its capacity [2]. In this investigation, 10 bar is set as initial pressure. Figure 2.2 shows how the initial pressure influences the dispensed hydrogen into the tank.

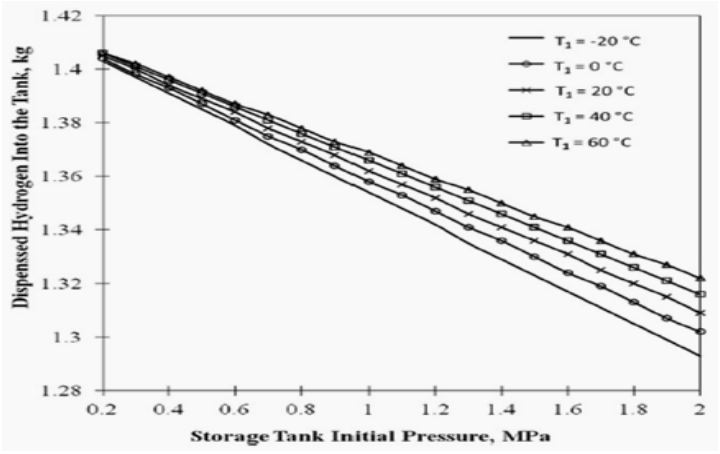

Figure 2.2: The trend of dispensed hydrogen into the tank versus initial pressure inside the tank[2]

2.3 Inlet temperature

There are some regulations in the refueling process making constraints in the inlet temperature. So, according to these regulations, the tank has to be designed for the range of -40 to 85°C. It means that the inlet temperature cannot be less than -40°C [4]. In some cases, in order to not exceed the temperature limitation (85°C), the inlet hydrogen is preferred to be precooled [2]. To be more accurate, the cold filling leads the final temperature and pressure decreases and consequently it protects the tank against high-temperature consequences [3].

2.4 Heat transfer

Heat transfer plays a significant role in the final temperature inside the tank and it is mainly depended on the type of the tanks. To be more accurate, there is a heat loss through the wall. The wall thickness and its conductivity influence the rate of heat transfer. Besides, the temperature differences between inside and outside the tank also determine this rate [1]. For calculating the heat transfer, the heat transfer coefficient between the wall of the tank and the air outside of the tank can be estimated from Equation (2.1)

$$h = 10.45 - v + 10v^{1/2} \tag{2.1}$$

where v is the relative speed between the wall and air [9]. Since in this investigation, it is assumed that the ambient air is stagnant and there is no wind in area, the heat transfer coefficient is equal to 10.45 W/(m^2·K).

2.5 Joule-Thomson effect

When compressed gas is expanded or released through a valve to lower pressure environment, in one hand, this leads the gas to heat up while the expansion itself cools the gas. These two mechanisms compete which are known as Joule-Thomson effect [10]. In general, it can be stated that Joule-Thomson coefficient is identified by the partial derivative of the pressure respect to temperature at constant enthalpy and Joule-Thomson effect is described by obtaining this coefficient [11]. For most kinds of gases in normal condition[1], the Joule-Thomson coefficient is positive which means that the gas is cooled during expansion while for few gases such as hydrogen it works in the other way around in the relevant range of pressure and temperature[2, 4]. In other words, when the tank is filled by hydrogen, as the gas is expanded after passing the nozzle, the temperature increases inside the tank. Figure 2.3 depicts the trend of Joule-Thomson coefficient versus temperature at atmospheric pressure for several gases including hydrogen.

[1] At 25°C and 1 atm

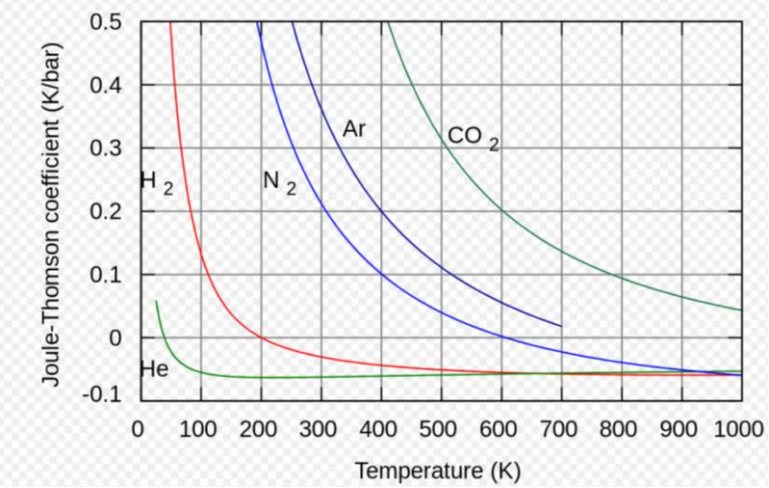

Figure 2.3: Joule-Thomson coefficient versus temperature at atmospheric pressure[12]

A further point to add is that when the tank is filled, the hydrogen is accumulated and compressed hence it is another reason for the increasing temperature inside the tank however it is necessary to clarify that the effect of compression during the filling is completely different from Joule-Thomson effect [2].

3 Theory of CFD

In this chapter, the theory of the relevant part of CFD used in this study has been discussed.

3.1 Transport Equation

The CFD equations are generalized in form of transport equation shown in Equation (3.1).

$$\frac{\partial(\rho\varphi)}{\partial t} + div(\rho\varphi\vec{\mathbf{u}}) = div(\Gamma grad\varphi) + S_{\varphi} \tag{3.1}$$

As a matter of fact, the Navier-Stokes equations plus internal energy equation can be extracted from the general form of transport equation which are shown in Equations (3.2).

$$\begin{cases} \dfrac{\partial\rho u}{\partial t} + \mathrm{div}(\rho u\mathbf{u}) = -\dfrac{\partial p}{\partial x} + \mathrm{div}(\mu\ \mathrm{grad}\ u) + S_{Mx} \\ \dfrac{\partial\rho v}{\partial t} + \mathrm{div}(\rho v\mathbf{u}) = -\dfrac{\partial p}{\partial y} + \mathrm{div}(\mu\ \mathrm{grad}\ v) + S_{My} \\ \dfrac{\partial\rho w}{\partial t} + \mathrm{div}(\rho w\mathbf{u}) = -\dfrac{\partial p}{\partial z} + \mathrm{div}(\mu\ \mathrm{grad}\ w) + S_{Mz} \\ \dfrac{\partial\rho i}{\partial t} + \mathrm{div}(\rho i\mathbf{u}) = -p\ div\ \mathbf{u} + \mathrm{div}(k\ \mathrm{grad}\ T) + \Phi + S_i \end{cases} \tag{3.2}$$

In addition, there are always fluctuations in velocity and pressure terms which can be considered as following terms:

$$\mathbf{u} = \mathbf{U} + \mathrm{u}' \qquad u = U + u' \qquad v = V + v' \qquad w = W + w' \qquad p = P + p'$$

By inserting these terms into Navier-Stokes equations being in Equations (3.2), Equations (3.3) are performed as follows:

$$\begin{cases} \dfrac{\partial\rho U}{\partial t} + \mathrm{div}(\rho U\mathbf{U}) = -\dfrac{\partial P}{\partial x} + \mathrm{div}\big(\mu\ \mathrm{grad}(U)\big) + \left[\dfrac{\partial\big(-\rho\overline{u^{2\prime}}\big)}{\partial x} + \dfrac{\partial(-\rho\overline{v'u'})}{\partial y} + \dfrac{\partial(-\rho\overline{u'w'})}{\partial z}\right] \\ \dfrac{\partial\rho V}{\partial t} + \mathrm{div}(\rho V\mathbf{U}) = -\dfrac{\partial P}{\partial y} + \ \mathrm{div}\big(\mu\mathrm{grad}(V)\big) + \left[\dfrac{\partial(-\rho\overline{v'u'})}{\partial x} + \dfrac{\partial\big(-\rho\overline{v^{2\prime}}\big)}{\partial y} + \dfrac{\partial(-\rho\overline{v'w'})}{\partial z}\right] \\ \dfrac{\partial\rho W}{\partial t} + \mathrm{div}(\rho W\mathbf{U}) = -\dfrac{\partial P}{\partial y} + \mathrm{div}\big(\mu\mathrm{grad}(W)\big) + \left[\dfrac{\partial(-\rho\overline{w'u'})}{\partial x} + \dfrac{\partial(-\rho\overline{v'w'})}{\partial y} + \dfrac{\partial\big(-\rho\overline{w^{2\prime}}\big)}{\partial z}\right] \end{cases} \tag{3.3}$$

These equations can be simplified by introducing Reynolds stresses defined as follows [13]:

$$\tau_{xx} = -\rho\overline{u'^2} \qquad \tau_{yy} = -\rho\overline{v'^2} \qquad \tau_{zz} = -\rho\overline{w'^2}$$

$$\tau_{xy} = \tau_{yx} = -\rho\overline{v'u'} \qquad \tau_{xz} = \tau_{zx} = -\rho\overline{w'u'} \qquad \tau_{yz} = \tau_{zy} = -\rho\overline{v'w'}$$

At last, it is necessary to add that the term S_φ in the general form of the transport equation represented the source of energy. In this investigation, the gravity force is considered as a source of energy.

3.2 Model of solving equations

In this part, some different models acquired by Reynold-Average Navier-Stokes (RANS) equation have been discussed briefly however the *k*- ε model used for this investigation has been explained in more detail.

As explained in Chapter 3.1, fluctuation causes extra terms added to the transport equations which means that more equations need to be enumerated in order to have the same number of unknowns and equations. To solve this problem, RANS is a proper choice and it is split into several models based on the number added equations [13].

As shown in Table 3.1, there are two variables solved in *k*-ε model. One is turbulent kinetic energy, ***k***, which determines the energy in the turbulence while the other one is turbulent dissipation, ***ε*,** depicting the scale of turbulence. This model has a wide range of convergence and does not require too much memory compared to other models. As a result, this is the most typical technique for turbulence models [14, 15].

Table 3.1: various models of RANS [13]

No. of extra transport equations	Name
Zero	Mixing length model
One	Spalart-Allmaras model
Two	*k*-ε model
	k-ω model
	Algebraic stress model
Seven	Reynolds stress model

When these extra variables are added, transport equations turn to Equations (3.4) and (3.5).

$$\frac{\partial(\rho k)}{\partial t} + div(\rho k \boldsymbol{U}) = div\left[\frac{\mu_t}{\sigma_k} grad\, k\right] + 2\mu_t S_{ij} \cdot S_{ij} + \rho\varepsilon \quad (3.4)$$

$$\frac{\partial(\rho \varepsilon)}{\partial t} + div(\rho \varepsilon \boldsymbol{U}) = div\left[\frac{\mu_t}{\sigma_\varepsilon} grad\, \varepsilon\right] + C_{1\varepsilon}\frac{\varepsilon}{k}\mu_t S_{ij} \cdot S_{ij} + C_{2\varepsilon}\rho\frac{\varepsilon^2}{k} \quad (3.5)$$

In these equations μ_t can be procured by Equation (3.6).

$$\mu_t = C_\mu \rho \frac{k^2}{\varepsilon} \quad (3.6)$$

Also, there are five adjustable constants in Equations (3.4), (3.5), and (3.6) where set in Table 3.2.

Table 3.2: The standard values of the constants of the *k*- ε model

C_μ	σ_k	σ_ε	$C_{1\varepsilon}$	$C_{2\varepsilon}$
0.09	1.00	1.30	1.44	1.92

In most cases, the values of *k* and ε are not available so it is possible to calculate them by Equations (3.7) and (3.8) [13].

$$k = \frac{2}{3}(U_{in} T_i)^2 \quad (3.7)$$

$$\varepsilon = C_\mu^{3/4} \frac{k^{3/2}}{l} \quad (3.8)$$

where

$$T_i = 0.16 Re^{\frac{-1}{8}} \qquad Re = \frac{UD}{\vartheta} \qquad l = 0.07L$$

3.3 Law of the wall

One of the factors that should be considered in the CFD simulation is the wall function because it contributes to finding the proper model and in consequence, acquire more accurate and trustable result. Law of the wall represents average velocity in a turbulent flow versus the

logarithmic distance from that certain point which is shown in Figure 3.1. There, y^+ and U^+ are the dimensional numbers representing the wall coordinate and the velocity respectively.

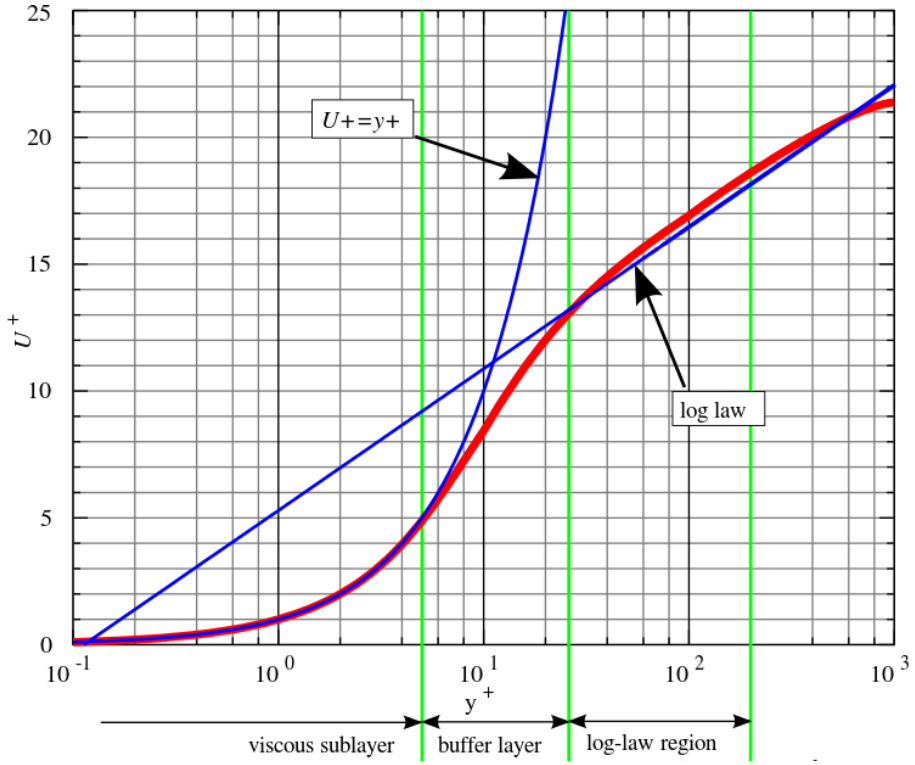

Figure 3.1: The diagram of the law of wall [16]

The red curve illustrates the experimental values which should be implemented in the simulation. Solving the equation which fits the exact values is time-consuming for many systems, so it is wise to find the simpler functions which depict in the blue lines. As can be seen, one of the blue lines is perfectly matched in the viscous sublayer while there is a good agreement for the other one in the log-law region. In the other words, the solution should be in either viscous sublayer or log-law region and it should be avoided to be in the buffer layer where $5<y^+<30$ [13, 16].

3.4 Finite Volume Method

The transport equations can be solved by developing numerical methods such as the Finite Volume Method. In this method, the whole solution domain is divided into a finite number of arbitrary control volumes or cells and the property of each cell stores in the middle point of that cell. It is worth knowing that the control volume can be formed in any shape (e.g., cubic, tetrahedrons, hexes and so on). Figure 3.2 depicts how a domain can be separated into the number of control volumes [13, 17].

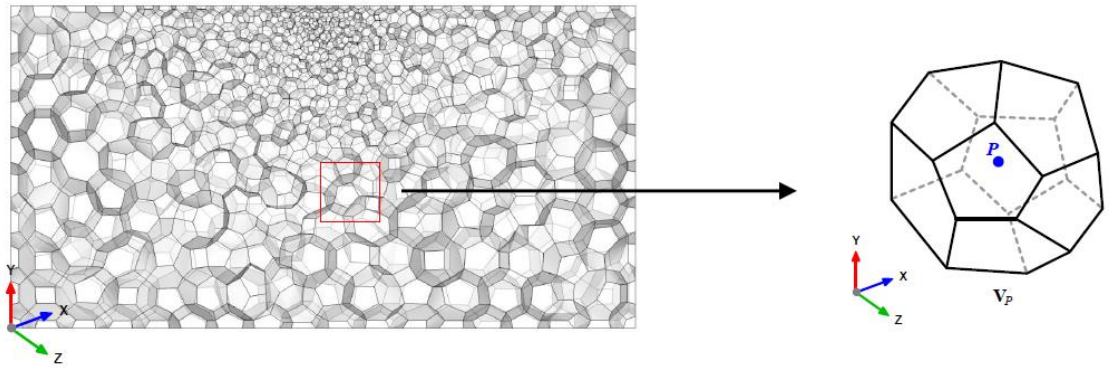

Figure 3.2: A sample of finite volume methods. The properties of each cell are stored it the point P [17].

3.5 Scheme

For choosing the proper scheme, it is necessary to know about the diffusion and convection terms and find out which term is dominated in the transport equation. This is possible by calculating the Peclet number shown in Equation (3.9).

$$Pe = \frac{U\delta x}{\acute{D}} \tag{3.9}$$

When the value of Peclet number is close to zero, it means that the diffusion term dominates the convection while the bigger the value of Peclet number is, the more convection there would be in the system. Later, in Chapter 4.4, it proves that convection dominates the diffusion in this investigation. This helps to choose the appropriate scheme. In other words, as there is more convection than diffusion, it is wise to use upwind scheme designed for such cases.

In the upwind scheme, as the cell faces are mostly influenced by the convection, the properties are inherited from the upstream node. In other words, if it is assumed that the direction of flow is positive (left to right) then [13]:

$$\varphi_w = \varphi_W \qquad\qquad \varphi_e = \varphi_P$$

Figure 3.3 contributes to understanding the concept easier.

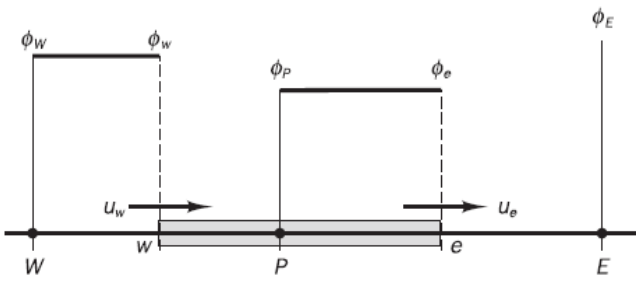

Figure 3.3: Example of nodes when the direction flow is positive [13]

3.6 Boundary Types

One of the important things in simulation is boundaries for both geometries and properties in order to create the mesh and set-up the simulation. Some basic and useful boundaries are introduced in Table 3.3 [18].

Table 3.3: Different types of the boundaries

Boundary Type	**Description**
patch	Generic type containing no geometric or topological information about the mesh e.g. used for an inlet or an outlet
wall	For patch that coincides with a rigid wall, required for some physical modelling
fixedValue	Value of the related property is specified by value
fixedGradient	Normal gradient of the property is assigned by gradient
zeroGradient	Normal gradient of the property is zero
calculated	The property is calculated from other patch fields

3.7 Solver

For solving the transport equations, there are several solvers. In this investigation, rhoCentralFoam has been used since it matches the case. This solver is density-based used for compressible flow. The different features including turbulence, transient, and heat transfer can be implemented in this solver which makes it a suitable one [13, 19, 20].

4 Simulation Set-Up

In this chapter, all detail which should be implemented in OpenFoam has been explained in the following sub-chapters.

4.1 Geometry and Size

First of all, for starting the simulation, the cylindrical tank supposed to be filled can be created in blockMesh. For this purpose, as can be seen in Figure 4.1, the geometry has been divided into five blocks which four of them are trapezoids while there is a square in the center. Then, the larger sides of trapezoids should be curved to transform into the circle. The same things have been performed to the sides of the square to turn it to the circle as well. The final geometry has ended up to the right picture of Figure 4.1 while the inner circle is the inlet which the diameter is variable, and the outer circle is the wall of the cylinder with 1.2 m diameter. It is good to know that the interfaces of trapezoids are merged automatically and have not been shown in the right picture. A further point to add is that the length of the cylinder is 12 meters. In Figure 4.2, the mesh of geometry in 3D is shown.

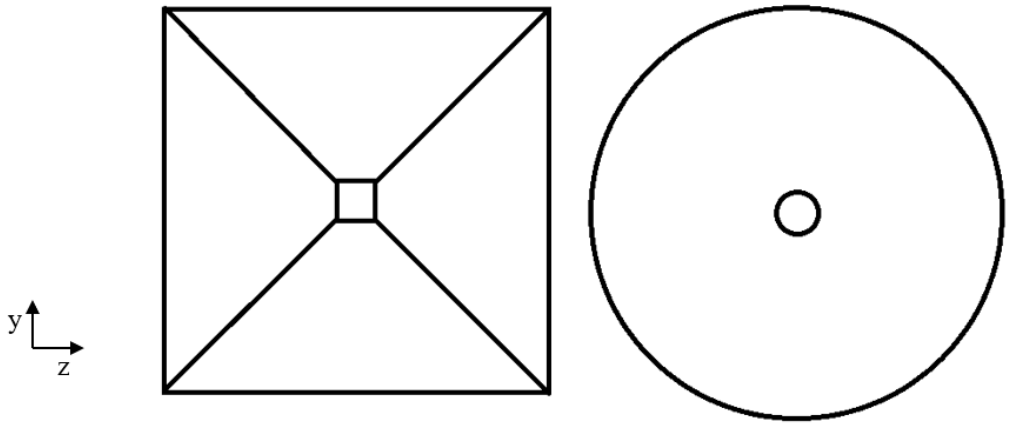

Figure 4.1: The blocks of cylinder created in blockMesh in 3D simulation

The way the volume is calculated is as following Equation (4.1):

$$V = \frac{ZmRT}{MP} \tag{4.1}$$

Where Z is the compressibility factor in 250 bar pressure and the 85°C temperature being 1.13347 [21] and M is the molecular weight of hydrogen being 2.016 g/mole. So, the final volume is:

$$V = \frac{1.13347 \cdot 200 \cdot 8.314 \cdot 358.15}{2.016 \cdot 10^{-3} \cdot 250 \cdot 10^{5}} = 13.3932\ m^3$$

Also, it is necessary to mention that the total geometry has 10,000 cells. Although it seems that it is not high resolution, this number of cells contribute to getting the result sooner. It would be possible to have finer mesh but that requires stronger systems. The mesh of the geometry is shown in Figure 4.2.

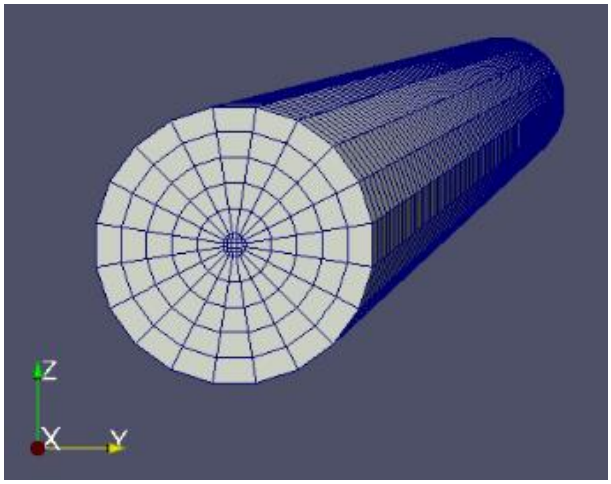

Figure 4.2: The mesh of 3D cylinder geometry

But even with decreasing the number of cells, 3D simulations are considerably time-consuming. Hence, that is why many simulations are preferred to be done in 2-dimensional instead. So, the geometry turns to a rectangle in 2D shown in Figure 4.3. It should be mentioned that all geometries in OpenFoam are 3D but with considering one cell in the z-direction, OpenFoam calculates all data in only two directions. A further point to add is that all sides are better to be kept as same as 3D to have more trustable data although one side should be sacrificed to keep the others adequate. In 2D geometry, the length is 12 meters and the height is 1.2 just as same as the 3D case but the width is set 0.93 meters to have the same volume as 3D has. The geometry and mesh of 2D of the cylinder is depicted in Figure 4.4.

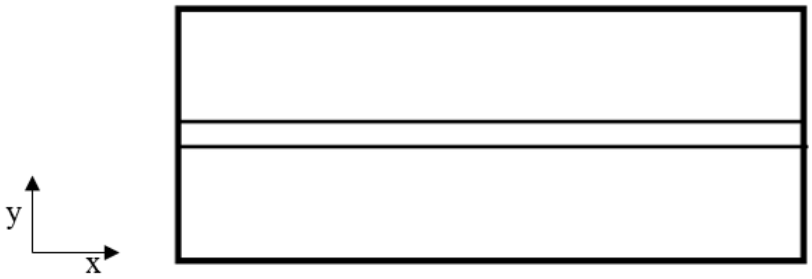

Figure 4.3: the blocks of hydrogen tank created in blockMesh in 2D

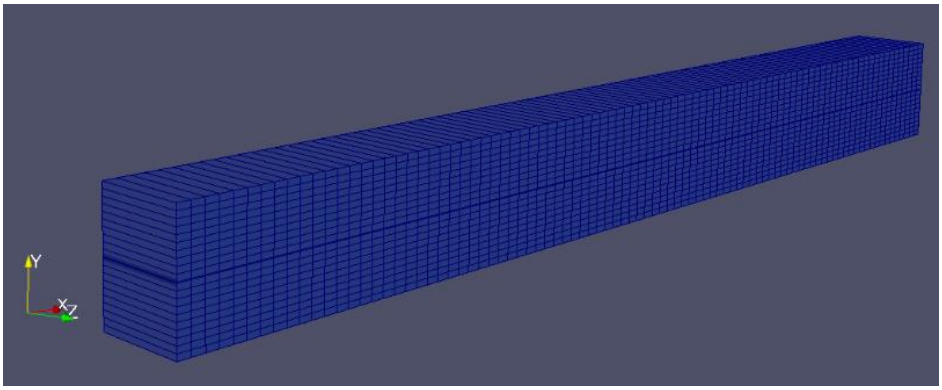

Figure 4.4: The 2D mesh of the cylinder

4.2 Cases

There are 5 cases simulated to investigate which are listed in Table 4.1. These cases have been created based on the diameter of the inlet, inlet temperature, the position of the inlet, and the number of dimensions.

Table 4.1: Different cases of simulation

Cases	Inlet diameter (m)	Inlet temperature (°C)	Inlet position	2D/ 3D
I	0.1	0	Left	3D
II	0.1	0	Left	2D
III	0.2	0	Left	2D
IV	0.2	-40	Left	2D
V	0.2	0	Top	2D

As mentioned in Chapter 4.1, the geometry in 2D is switched from the cylinder to the rectangular cubic. As a result, the geometry of the inlet in 2D is also a rectangle and not a circle. Hence, the inlet diameter in Table 4.1 identifies the equivalent diameter in 2D cases. In other words, the area of the rectangle is equal to the area of the assumptive circle with the equivalent diameter.

4.3 Boundary Condition

In this chapter, the initial condition of different thermodynamic properties has been discussed. The initial condition is mostly based on the condition set at the beginning for the system.

4.3.1 Temperature

The inlet temperature is different in cases mentioned in Table 4.1 while the initial temperature is constant in all cases being 25°C. So is the ambient temperature. Besides, as mentioned in Chapter 2.4, heat transfer also influences the simulation so all parameters should be inserted in simulation put in Table 4.2.

Table 4.2: The required parameters for simulating the heat transfer through the wall

Wall thickness [mm]	Thermal conductivity of wall [W/m·K]	Ambient temperature [°C]	Heat convection coefficient [W/m^2·K]
57	0.74	25	10.45

It is necessary to add that the heat convection coefficient between the hydrogen gas inside the tank and the wall is calculated automatically by OpenFoam itself while the heat convection coefficient in Table 4.2 is regarding the wall and ambient air calculated based on Equation (2.1). It is assumed that the air outside the tank is statistic and there is no wind.

A further point to add is that wall thickness and the related thermal conductivity is estimated based on a similar investigation done by K. Johnson et al [22].

4.3.2 Pressure

The inlet pressure of the tank increases during the filling process which should be considered in the simulation. The best solution is to put the experimental data of the inlet pressure as a function for simulation, but the problem is that in most cases, there is no such data. So according to what Galassi et al suggested, it is possible to make some alternative pressure profiles for the inlet pressure depicted in Figure 4.5. Although the best alternative can be different in various cases, a constant rise rate (which is almost similar to experimental data in Figure 4.5) is preferable in most cases [3].

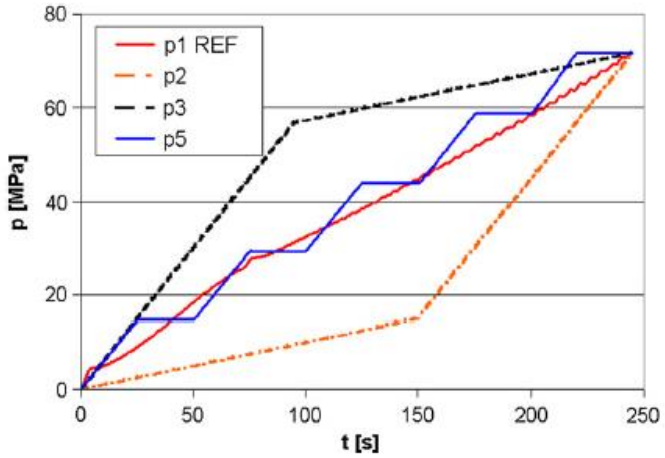

Figure 4.5: The inlet pressure profiles: the red line is fitted based on the experimental data which is similar to constant rise rate pressure profile[3]

In this investigation, it is assumed that the initial pressure is 10 bar while it is supposed to reach 250 bar. This should happen when the tank is filled with 200 kg of hydrogen. So, the amount of hydrogen in the tank should be calculated as introduced Equation (4.1) while the compressibility factor is considered one because it can be assumed that there is an ideal condition due to low pressure. Therefore:

$$m = \frac{MPV}{RT} = \frac{2.016 \cdot 10^{-3} \cdot 10^{6} \cdot 13.3932}{8.314 \cdot 298.15} = 10.89\ kg$$

This means that there is 189.11 kg of hydrogen which should be added to fulfill destiny. As the inlet mass flow is 1 kg/s, it takes 189.11 seconds to reach the desired final pressure. Hence, as discussed at the beginning of this chapter, the inlet pressure should increase gradually from 10 bar at the beginning to 250 bar at the end time shown in Figure 4.6.

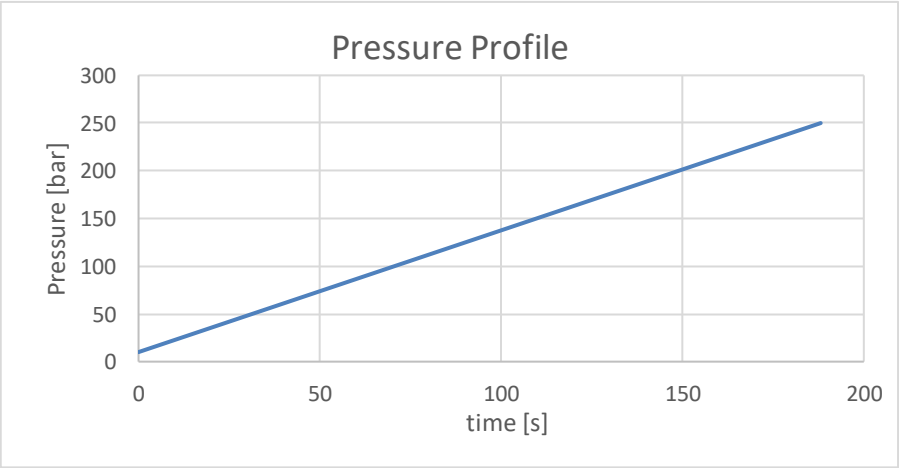

Figure 4.6: The inlet pressure profile used in this investigation

4.3.3 *k* and epsilon

The values of *k* and epsilon can be calculated from Equations (3.7) and (3.8) inserted in Table 4.3.

Table 4.3: Values of *k* and epsilon for different cases

Case	k [m²/s²]	epsilon (ε) [m²/s³]	U [m/s]
I	10.14	757.77	144.33
II	18.85	22952.26	144.33
III	1	36.11	36.08
IV	0.7	21.36	30.73
V	1	36.11	36.08

It is necessary to admit that for calculating these values, first the values of density and dynamic viscosity from the trustable sources put in Appendices A and B should be extracted and then the inlet velocity at the beginning of the process can also be procured by Equation (4.2).

$$U = \frac{\dot{m}}{\rho A} \tag{4.2}$$

4.3.4 Velocity

Mainly, the inlet velocity has been assigned at the beginning by the user but in this investigation, the inlet mass flow has been set instead and the inlet velocity would be calculated by the software itself, however, the inlet velocity has been calculated in chapter 4.3.3 and it is later possible to compare those results to the inlet velocities obtained by the OpenFoam.

4.4 fvSchemes

In chapter 3.5, it has been represented that upwind scheme is used for this investigation. Here, numerically, it will be proved that this scheme is a proper one to calculate properties of each cell. For this purpose, the Peclet number should be calculated and the value of Peclet number indicates the proper scheme. The Peclet number of Case I is calculated below as an example by using Equation (3.9). It is necessary to admit that although calculating the Peclet number for other cases give different values, they are still big enough to prove the same claim.

$$Pe = \frac{U\delta x}{\acute{D}} = \frac{144.33 \cdot 0.002}{1.6 \cdot 10^{-8}} = 1.8 \cdot 10^{7}$$

As the value of the Peclet number is big, it can be concluded that the convection source dominates the diffuse terms and that is why the upwind is a suitable scheme for this and other cases. It is better to add that in the equation above, $\acute{D}$ is the self-diffusion of hydrogen being 1.6e-8 [23], U is the velocity of the hydrogen and the δx is cell width which is 0.002 meters in the smallest one.

4.5 Thermodynamic Properties

Thermodynamic properties are the ones needed to be inserted into the program. In this case, the specific heat is not a constant number and it depends on the temperature otherwise the Joule-Thomson effect cannot be observed. This property beside enthalpy and entropy can be acquired from the Nasa Polynomials which are presented in Equations (4.3).

$$\begin{cases} C_p/R = a_1 + a_2T + a_3T^2 + a_4T^3 + a_5T^4 \\ H/RT = a_1 + a_2T/2 + a_3T^2/3 + a_4T^3/4 + a_5T^4/5 + a_6/T \\ S/R = a_1\,lnT + a_2T + a_3T^2/2 + a_4T^3/3 + a_5T^4/4 + a_7 \end{cases} \quad (4.3)$$

Where the coefficients are available in Table 4.4.

Table 4.4: Nasa Polynomial Coefficients for hydrogen (H_2)

Range of temperature (K)	**a_1**	**a_2 ($\cdot 10^{-5}$)**	**a_3 ($\cdot 10^{-7}$)**	**a_4 ($\cdot 10^{-10}$)**	**a_5 ($\cdot 10^{-14}$)**	**a_6**	**a_7**
200-1000	3.33727920	-4.94024731	4.99456778	-1.79566394	2.00255376	-950.158922	-3.20502331
1000-3500	2.34433112	798.052075	-194.781510	201.572094	-737.611761	-917.935173	0.683010238

It is necessary to admit that the Coefficients in Equations (4.3) have different values in a different range of temperatures [24].

In the next step, dynamic viscosity (μ) and thermal conductivity (k) should be calculated by the software itself. Dynamic viscosity can be calculated by Equation (4.4).

$$\mu = \frac{A_s\sqrt{T}}{1 + T_s/T} \quad (4.4)$$

In the equation above, A_s is the Sutherland coefficient while the T_s is the Sutherland temperature being 6.362e-07 $\frac{kg}{ms\sqrt{K}}$ and 72 K respectively [25-27].

Then, thermal conductivity can be obtained by Equation (4.5). There, C_p and μ are obtained by Equations (4.3) and (4.4) while the Prandtl number is 0.69 for hydrogen [25, 28].

$$k = \frac{C_p \mu}{Pr} \tag{4.5}$$

5 Result and Comparison

In this chapter, all results for all cases mentioned in Table 4.1 are shown and analyzed. Simultaneously, these cases are compared to each other to reveal the impact of changing the diameter, inlet temperature, and the position of the inlet. Also, the results between 2D and 3D simulations are discussed.

5.1 3D vs 2D (Case I vs Case II)

Looking deeply in Table 4.1 reveals that all parameters for Case I and Case II are the same. The only difference is that Case I is implemented in 3-dimension while Case II is in 2-dimension. Hence, it is expected that both cases have more and less similar results and trends.

Figure 5.1 depicts that the temperature inside the tank increases and becomes stable in 388 K and 368 K in 2D and 3D cases, respectively. This means that there is about 5% error which seems acceptable.

The reason for this trend comes from the impact of compression, Joule-Thomson effect, and the heat transfer between the hydrogen and the ambient air through the wall of the tank. First, when the hydrogen is dispensed to the tank, the temperature increases due to the effect of compression and also Joule-Thomson coefficient. However, the temperature becomes stable after a while since the rate of heat transfer between the hydrogen and the air outside becomes almost equal to those effects. To be more deep in Figure 5.1, it reveals that the temperatures decrease very smoothly at the end which shows that the effect of heat transfer becomes greater while the Joule-Thomson coefficient and compression have less effort during the time.

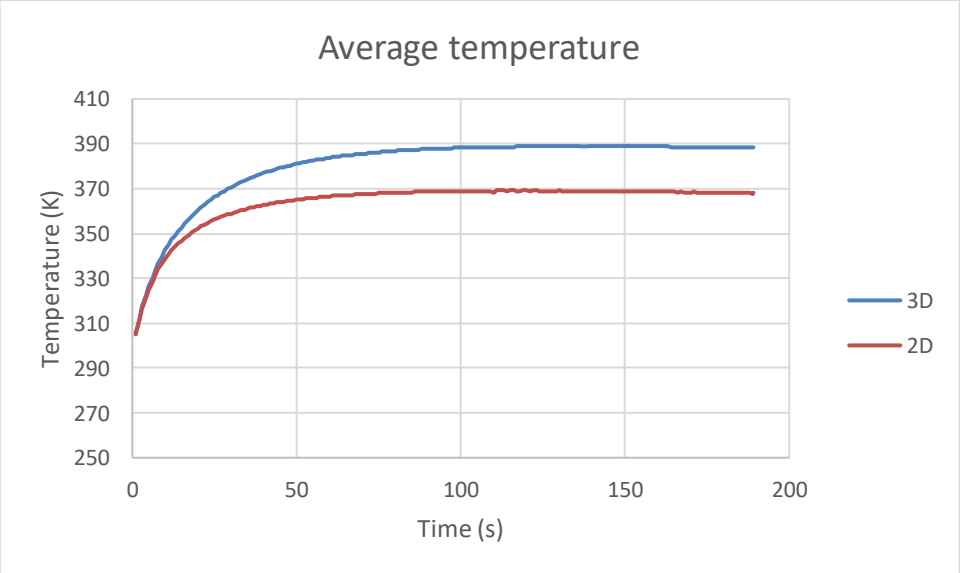

Figure 5.1: Average temperature inside the tank in each time step for Case I (3D) and Case II (2D)

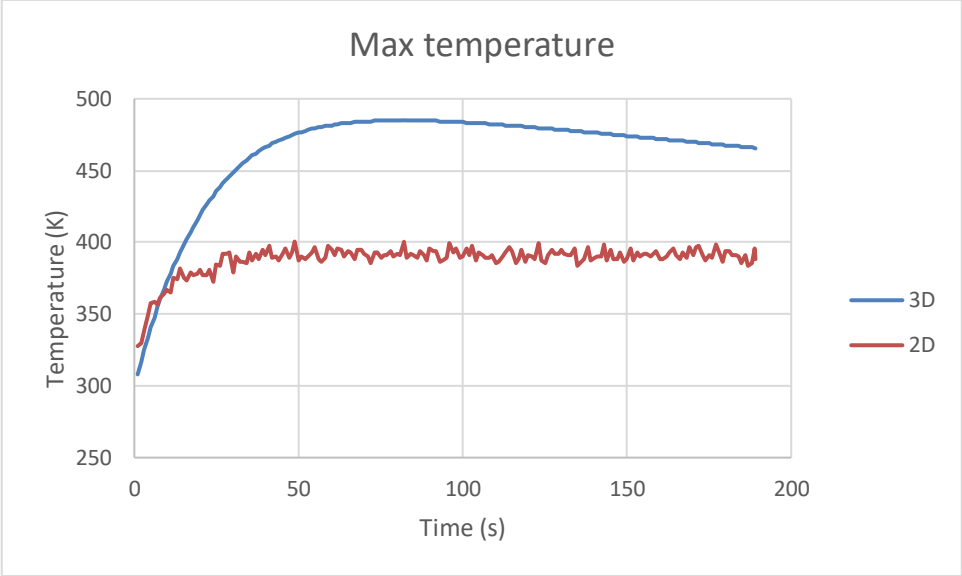

Figure 5.2: The trend of maximum temperature for the Case I (3D) and Case II (2D) during the time

Also, as shown in Figure 5.2, the maximum temperature increases in general. In 3D case, it grows until it reaches 485 K and decreases slowly afterward while in 2D case, it raises for a while and then it starts fluctuation between 385 and 401 K. Figure 5.3 contributes to understanding this weird behavior in 2D.

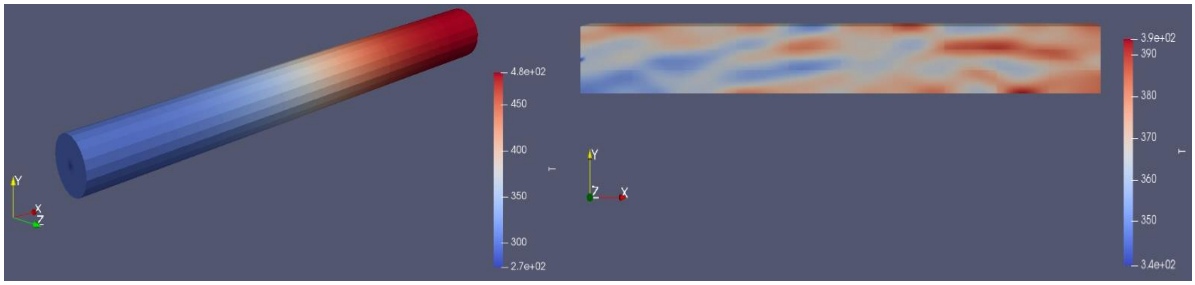

Figure 5.3: Temperature profile in 3D (left picture) and 2D (right picture) at the 92nd second

As a matter of fact, in 3D, the calculation is done in three dimensions and as seen in Figure 5.3, the temperature is distributed in the whole domain perfectly while in 2D, the temperature field is heterogeneous. This interpretation can be done by considering the values of *k* and epsilon at a certain time (e.g. 92nd second).

Table 5.1 reveals that these values are greater in 2D compared to 3D which means that the variation of temperature during the time is considerable at each cell in 2D. That is why the temperature distribution is not homogenous in neighbor cells and each cell's temperature may change dramatically in each time step in 2D. Also, comparing Figure 5.3 to Figure 5.4 discloses that the temperature profile in 3D is almost stagnant after one second while this can be extremely different in 2D at the same time steps.

Table 5.1: The average values of *k* and epsilon in the whole domain at 92nd second

	k [m²/s²]	**epsilon (ε) [m²/s³]**
Case I	0.051	0.81
Case II	9.007	35.17

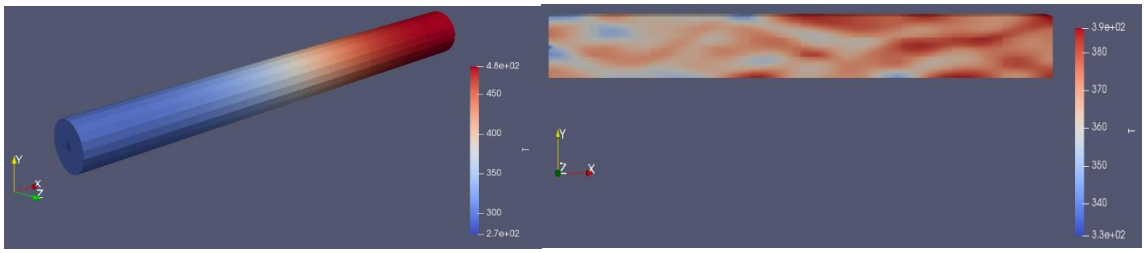

Figure 5.4: Temperature profile in 3D (left picture) and 2D (right picture) at the 93rd second

In addition, pressure is another parameter to consider. As shown in Figure 5.5, the pressure in both cases follows the same patent and the values are way too close to each other.

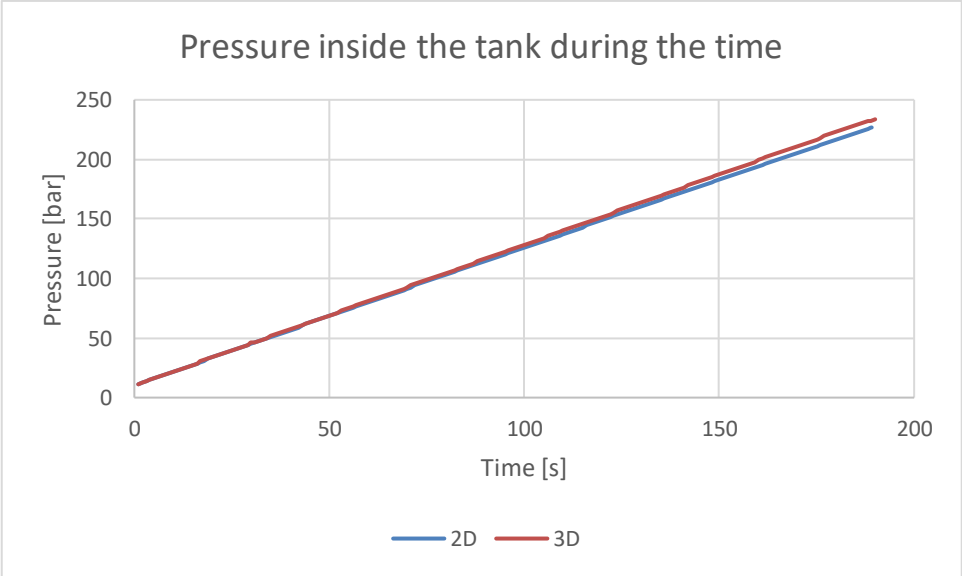

Figure 5.5: Comparison of pressure between Case I and Case II

5.2 Impact of changing the inlet diameter (Case II vs Case III)

First, it is necessary to admit that in all 2-dimensional cases, the calculation of the inlet area has been done base on the 3-dimensional one. In other words, as the inlet area in 2-dimension is a rectangle, the effect of changing the diameter in 3-dimension reveals in changing the area

in 2-dimension. Hence, as the diameter of Case III is twice as big as Case II, the area is four times bigger.

Figure 5.6 and Figure 5.7 disclose how increasing the diameter affects the temperature inside the tank. The trend of temperature behavior in Case III is as what was discussed for Case II. The difference is that the average temperature in Case III is 8 K higher reaching 377 K at the end while the maximum temperature in Case III is 6 K less, being 395 K.

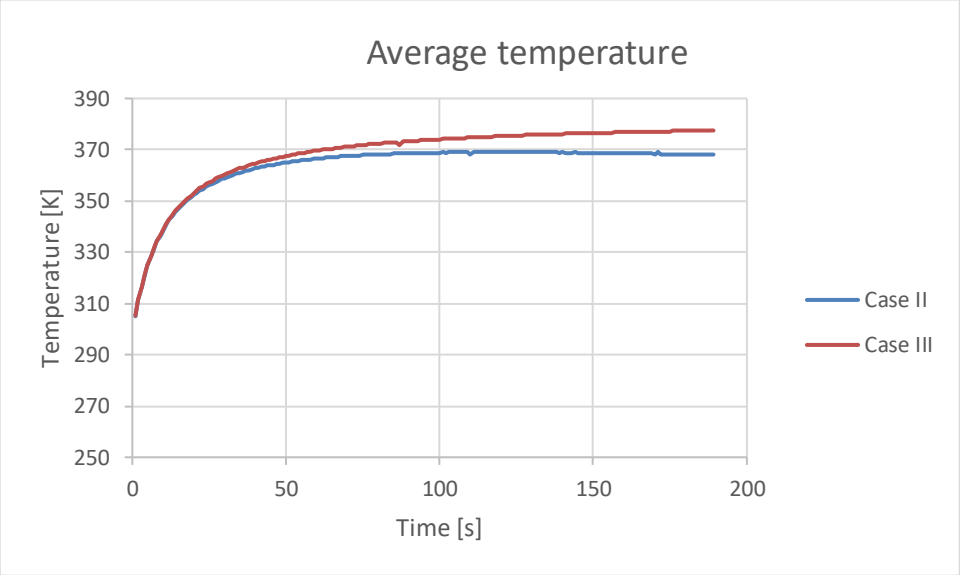

Figure 5.6: Average temperature inside the tank in each time step for Case II and Case III

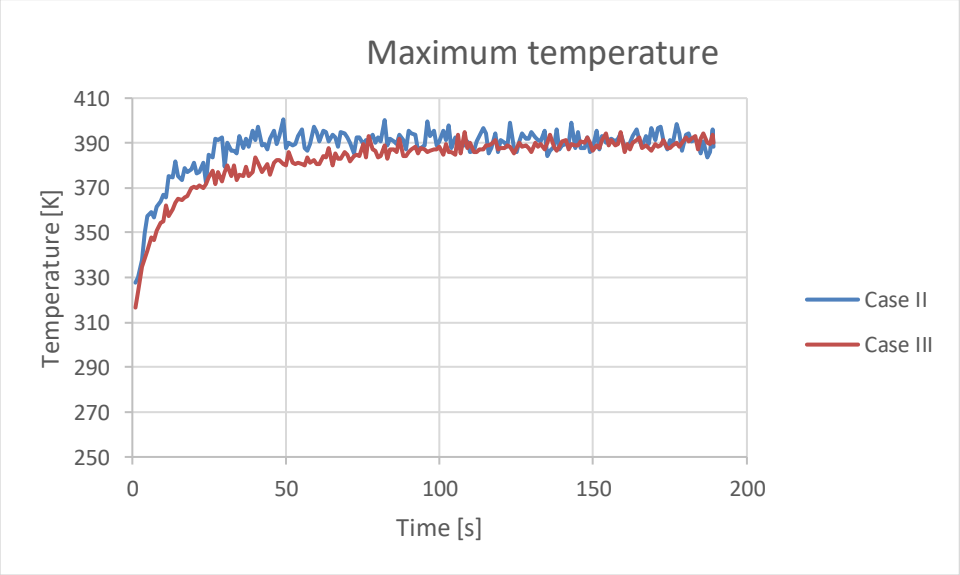

Figure 5.7: The trend of maximum temperature for Case II and Case III during the time

To be more deeply, as seen in Figure 5.7, the maximum temperature in Case II grows faster first and then becomes similar to Case III. This can be analyzed by discussing inlet velocity. The inlet velocity calculated and put in Table 4.3 reveals that there is higher inlet velocity in Case II which causes the momentum. Besides, the value of epsilon is also considerable. As a result, the kinetic energy produced due to momentum is dissipated and transformed into the heat. During the time, the inlet velocity decreases so, the value of the maximum temperature of both cases becomes closer.

In contrast, the average temperature in Case III is higher while they are almost the same at the beginning. The reason can be searched in the final average velocity and also the final value of *k* and epsilon in the tank which is shown in Table 5.2. As seen, the final velocity in Case III is greater and at the same time, the value of epsilon is considerably bigger which causes more energy to be transformed to heat.

Table 5.2: Final values of *k*, epsilon and the velocity in the tank for Case II and Case III

	k [m^2/s^2]	epsilon (ε) [m^2/s^3]	U [m/s]
Case II	8.921	34.7	5.2
Case III	5813	595564	7.8

A further point to add is that as both cases have big values of *k* and epsilon, it is expected that the temperature profile would be messy shown in Figure 5.8. To be more accurate, the hot points in Case II are mostly at the end of the cylinder while in Case III, these red points are distributed in the whole domain can be also seen near the inlet since Case III has greater values of *k* and epsilon.

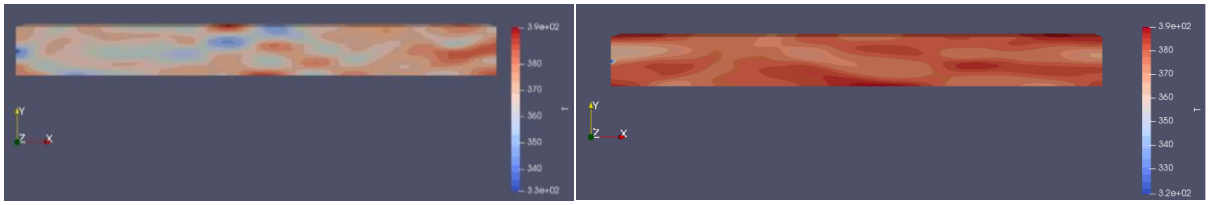

Figure 5.8: Temperature profile in Case II (left picture) and Case III (right picture) at the final time step

5.3 Impact of inlet temperature (Case III vs Case IV)

As shown in Figure 5.9 and Figure 5.10, decreasing the inlet temperature leads to having smaller average temperature and also maximum temperature. In Case IV, the maximum temperature is 340 K while the average temperature reaches 326 K. This is exactly what could be expected but the point is that the temperature difference is 40 K at the beginning while this difference grows to about 60 K.

The reason stems from the inlet velocity. To be more accurate, in Case III, higher momentum and in other words more kinetic energy is injected into the system which causes heating up the hydrogen inside the tank.

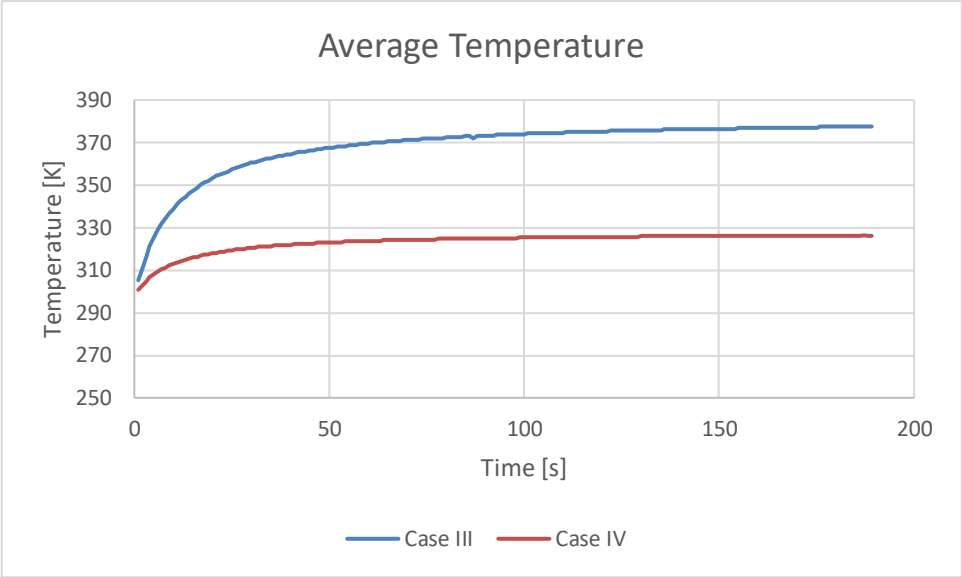

Figure 5.9: Average temperature inside the tank in each time step for Case III and Case IV

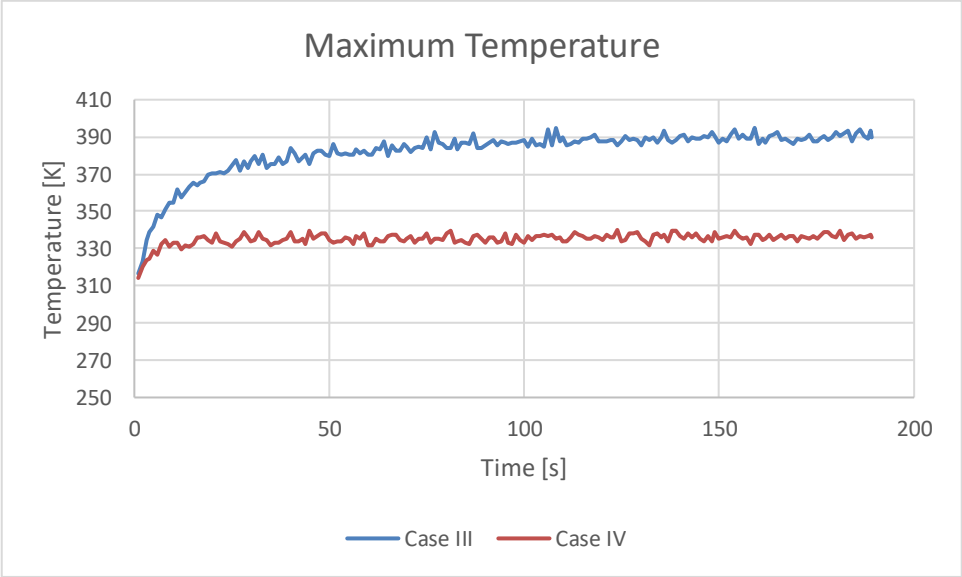

Figure 5.10: The trend of maximum temperature for Case III and Case IV during the time

At last, it is worthy to know how changing the inlet temperature affects the values of *k* and epsilon. As given in Table 5.3, these values are still big however they are smaller than Case III so, the temperature field of Case IV is more and less similar to Case III shown in Figure 5.11.

Table 5.3: Final values of k and epsilon in the tank for Case IV

	k [m²/s²]	epsilon (ε) [m²/s³]
Case IV	3929	335749

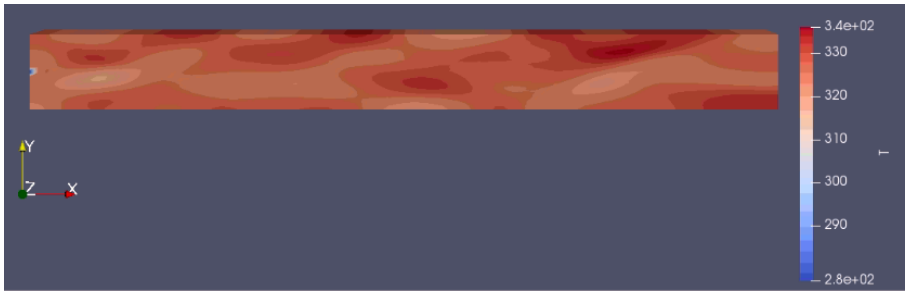

Figure 5.11: Temperature profile of Case IV at the final step

5.4 Impact of changing the inlet position (Case III vs Case V)

As shown in Figure 5.12 and Figure 5.13Figure 5.13, changing the inlet position influences the temperature inside the tank dramatically. In other words, when the inlet position is placed at the top of the tank (Case V), both average and maximum temperatures have significant growth.

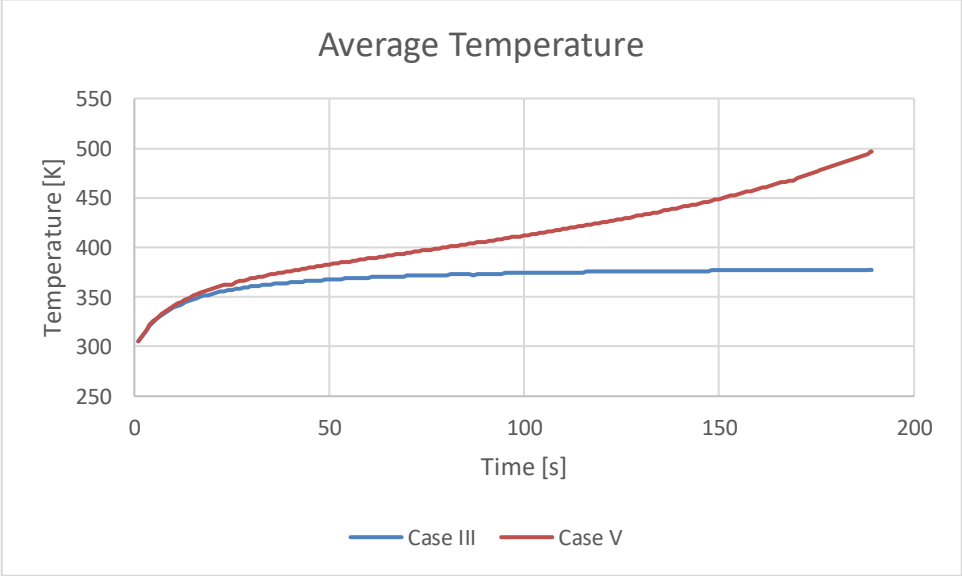

Figure 5.12: Average temperature inside the tank in each time step for Case III and Case V

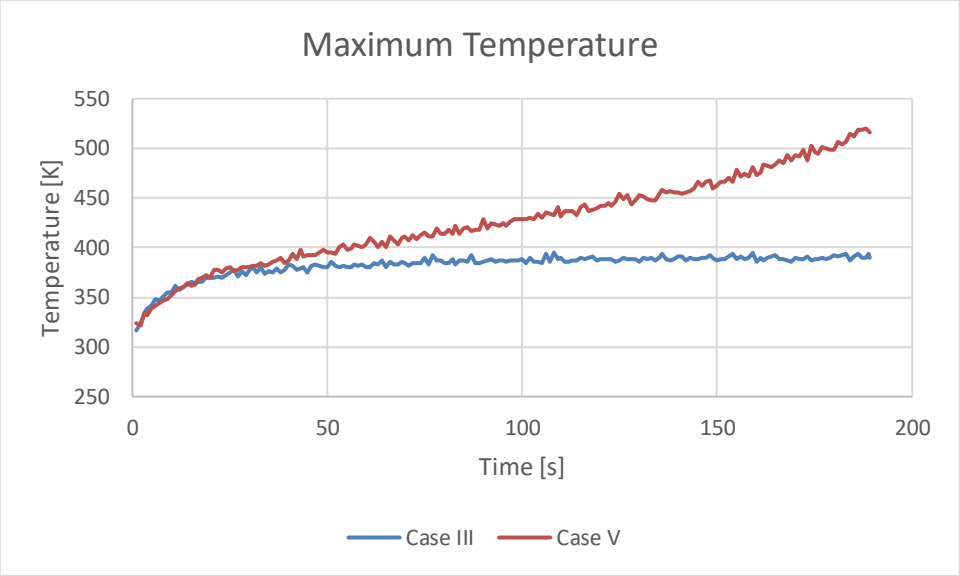

Figure 5.13: The trend of maximum temperature for Case III and Case V during the time

In Case V, the distance between the inlet and the front wall of the inlet is shorter compared to Case III. As a matter of fact, the wall acts as a ban and since the inlet hydrogen is hit to the wall with higher velocity, the turbulence increases and as a result, the level of energy in the tank grows and at the same time the amount of dissipation rises. This interpretation can be proved by checking the value of *k* and epsilon at the end of the process put in Table 5.4.

Table 5.4: Final values of *k* and epsilon in the tank for Case III and Case V

	k [m^2/s^2]	epsilon (ε) [m^2/s^3]
Case III	5813	595564
Case V	19079	3775580

As seen in Table 5.4, there is considerable growth in the amount of dissipation which explains this temperature difference between Case III and Case V. Besides, as these values are big, it can be expected that the temperature profile would be like other 2D simulations depicted in Figure 5.14.

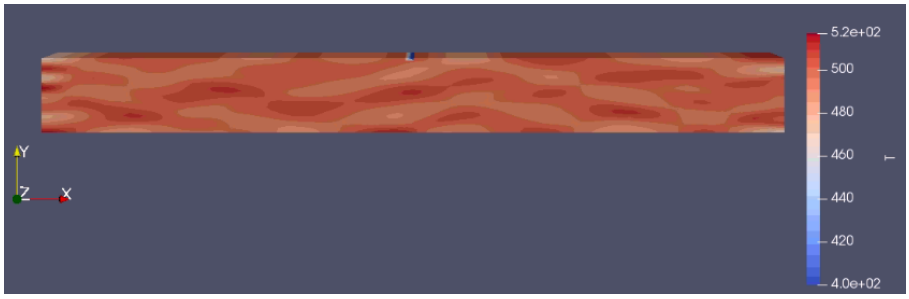

Figure 5.14: Temperature profile of Case V at the final step

5.5 Considering the temperature regulation

As discussed in Chapter 1, the temperature of the hydrogen should not exceed 85 °C (358.15 K). This regulation is investigated in Figure 5.15. As seen, in all cases but Case IV the maximum temperature exceeds the regulation which means that the 0°C inlet temperature is not suitable to avoid exceeding the regulation. In other words, only Case IV with -40 °C inlet temperature can be implemented in industries.

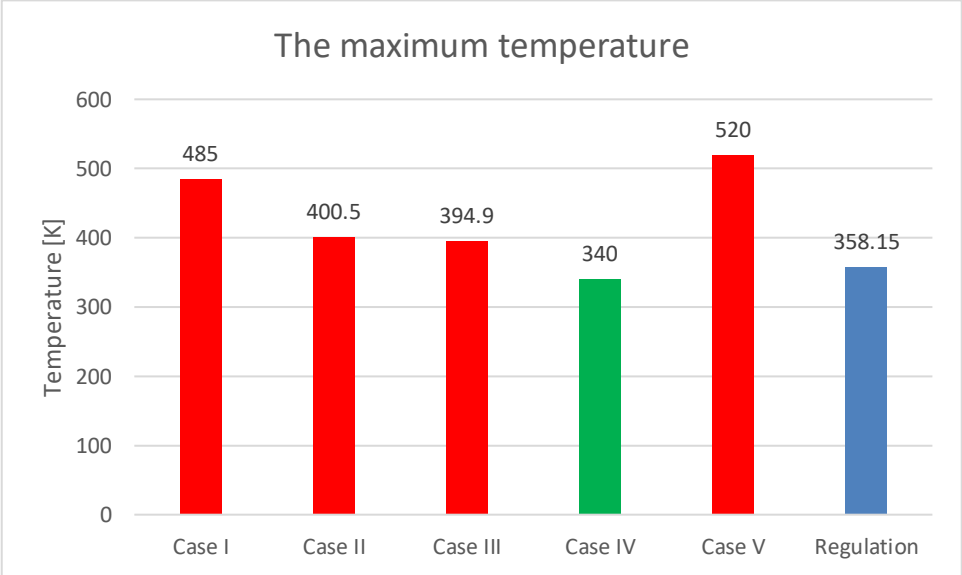

Figure 5.15: Comparing the temperature regulation to maximum temperature in all cases

5.6 Validating the results

Generally, the simulation results are validated with experimental data or other simulation software. Since there is no experimental or simulation data in this investigation, it cannot be guaranteed that the results would be matched perfectly with experimental data but it is possible to compare the final results to what was expected, estimated, or calculated.

First, as discussed in Chapter 4.3.2, the hydrogen mass inside the tank should reach 200 kg. Therefore, it is necessary to check that if this happens which is done in Figure 5.16. As seen, the final mass in all cases is way too close to what was expected.

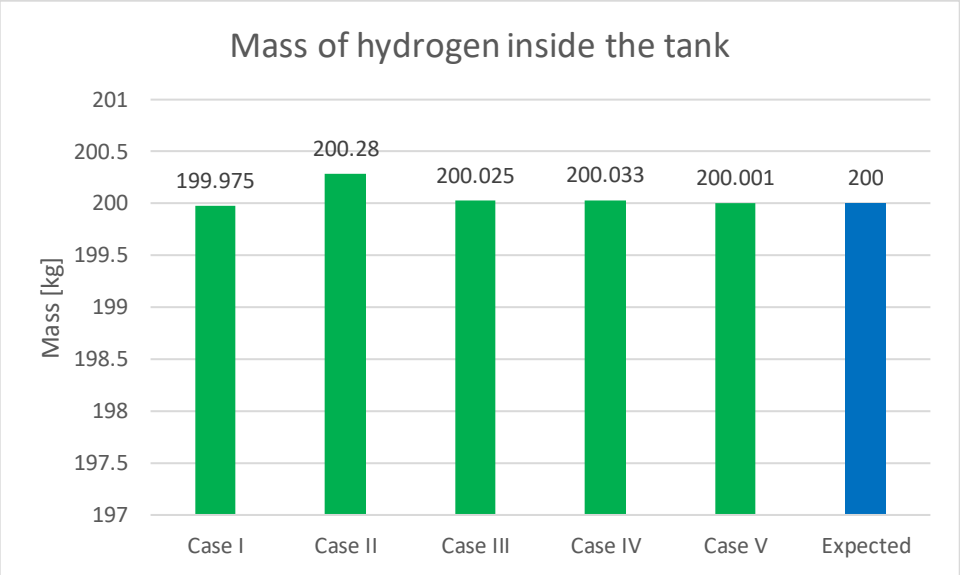

Figure 5.16: Hydrogen mass in all cases compared to the expected one

The other factor to consider is the final pressure. As explained in Chapter 4.1, it was estimated that the pressure reaches about 250 bar if it is assumed that the final average temperature inside the tank would be 85 °C. Since the final temperature in none of the cases is 85 °C (358.15 K), the final pressure should be different from what was calculated but the difference should be rational. The final pressures in all cases are shown in Figure 5.17 while the final average temperatures are listed in Table 5.5.

Looking deeply at Table 5.5 discloses that in all cases but Case IV, the final average temperature is more than 358.15 K. Hence, it can be deduced that the final pressure should be more than 250 bar while Figure 5.17 shows the opposite. The reason stems from the existence of the compressibility factor (z) in the calculation while this term was ignored in the simulation. In other words, it was assumed that the hydrogen is a real gas so all calculation in the simulation was done by this assumption. It was possible to implement the Peng-Robinson equation of state to consider the compressibility factor but this would be time-consuming since this factor should be calculated in each cell and in each time step.

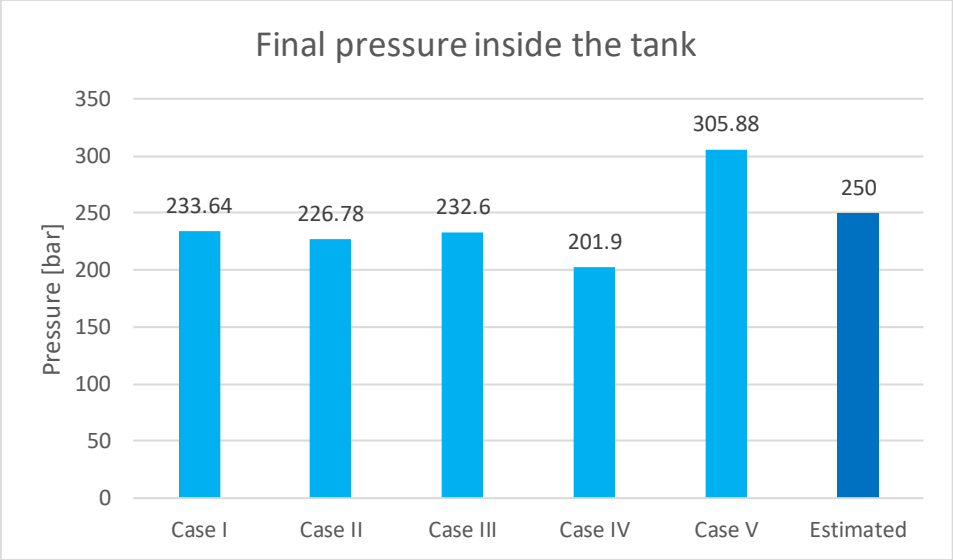

Figure 5.17: Comparing the final pressure inside the tank to the estimated pressure

Table 5.5: Final average temperature in all cases

	Case I	Case II	Case III	Case IV	Case IV
Final average temperature [k]	388.3	368	377.5	326.4	496.5

But, if the compressibility factor is considered only in the last time step (or in other words, the final pressure is multiplied by compressibility factor), the final pressures would end up with the results set in Figure 5.18.

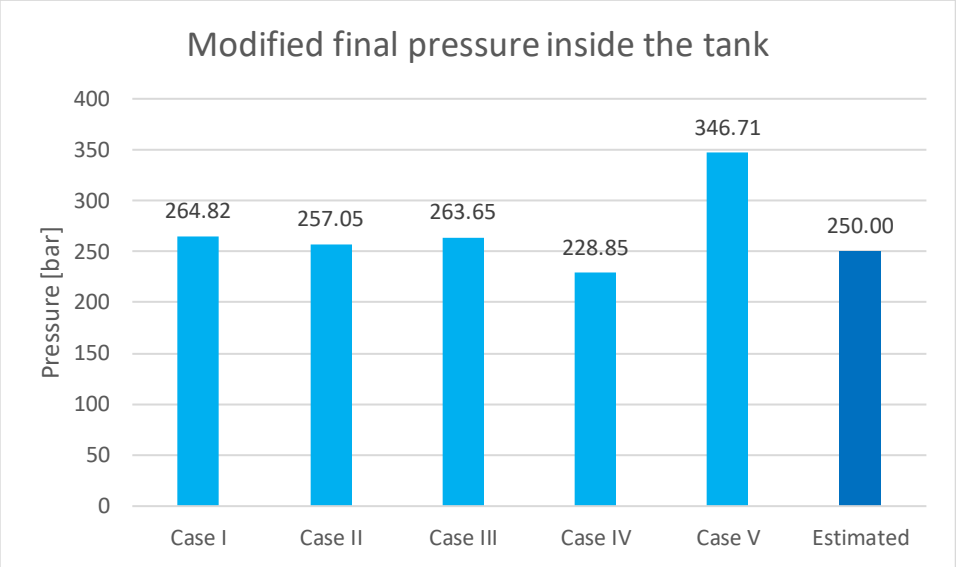

Figure 5.18: Final pressure by considering the compressibility factor versus the estimated pressure

Now it can be seen that the results are reasonable since when the average temperature is more than 358.15 K, the final pressure is also more than 250 bar as expected.

6 Conclusion

Hydrogen as a sustainable carbonless energy carrier is one of the most important targets to invest in. Because of that, this project deals with the difficulties of refueling the hydrogen inside the tank concerning some regulations. The most important issue is the maximum temperature which should not reach 85°C (358 K) due to avoiding embrittlement in the wall of the tank.

This investigation was done by the assumption of constant mass flow (1 kg/s) and constant ambient temperature (25°C) while the hydrogen inside the tank has the pressure of 10 bar and the temperature of 25°C initially.

OpenFoam was established to perform the different cases for this project by making the geometry in blockMesh both in 2D and 3D. Proper boundary types and inputs are set-up in the simulation to implement the cases.

According to the results acquired by the simulation, first of all, the inlet temperature must be precooled to fulfill the temperature regulation otherwise the temperature would exceed 85°C. Hence, it seems that Case IV with the inlet temperature of -40°C is proper to implement in reality however it seems that the inlet temperature can be a bit higher since the maximum temperature in Case IV reaches 67°C.

The position of the inlet is one of the most considerable issues for refueling since it can change the temperature significantly. It can be deduced that the vector of inlet velocity should be aligned with the length of the cylinder. This helps to have less kinetic energy and in consequence less dissipation in the system during the time because dissipation causes the kinetic energy transformed into the heat.

Another factor to consider is the inlet diameter or in better words, the inlet area. It can be deduced that in general the bigger the diameter, the higher the temperature is on average. However, this is the opposite for the max temperature. Besides, the greater inlet area causes bigger values of k and epsilon and as a result, the temperature distribution is not done adequately inside the tank. Although the most important factor in temperature distribution pertains to the number of dimensions' calculation, the effect of the inlet area cannot be ignored.

In general, it is possible to interpret the temperature differences between cases by Equation (6.1) if only just one parameter is changed.

$$f_{i,j} = \frac{\varepsilon_i}{\varepsilon_j} - \frac{k_i}{k_j} \tag{6.1}$$

Or in words:

$$f_{i,j} = ratio\ of\ epsilon\ in\ Case\ i,j\ -\ ratio\ of\ k\ in\ Case\ i,j$$

To be more accurate, the Equation (6.1) identifies the effect of kinetic energy and dissipation. If the effect of dissipation is greater than the effect of kinetic energy, the value of f becomes positive which means that the final temperature in Case i would be bigger than the temperature in Case j. In other words, the value of k and epsilon compete for assigning the final temperature.

To be more deeply, the greater the *k*, the smaller the temperature would be while in contrast, there would be higher temperature if the value of epsilon grows. Also, this equation probably works for each cell in each time step if the value of that cell and that time step is available.

7 Further Study

As there is a considerable investment in hydrogen tank refueling these days, it will have an interesting outlook. As a result, in this part, some tips are recommended to develop this study.

- **Implementing all 2D simulations in 3D**: This can contribute to having more trustable results although it takes more time and it requires a stronger system
- **Doing mesh independence**: This is also time-consuming and needs a quite powerful system but it improves accuracy.
- **Changing the sizes of geometry by keeping the same volume**: This is good to be investigated in order to find out how the length of the cylinder influences the temperature.
- **Establishing Peng-Robinson Equation of State**: It is worthful to do it for at least one of the cases and compare it to real gas equation of state.
- **Cooling the tank initially**: It is good to run a simulation when the hydrogen inside the tank is precooled and observe how it would affect the results.
- **Attempting to implement these cases in another software**: This helps to compare the results to what was obtained. Ansys Fluent can be a good alternative software.
- **Experimenting**: At last, it seems necessary to pick out one of the best and safest cases to perform in the laboratory in order to have some experimental results. This also helps to validate the simulation results.

References

[1] I. Simonovski, D. Baraldi, D. Melideo, and B. Acosta-Iborra, "Thermal simulations of a hydrogen storage tank during fast filling," *international journal of hydrogen energy*, vol. 40, no. 36, pp. 12560-12571, 2015.

[2] M. Hosseini, I. Dincer, G. Naterer, and M. Rosen, "Thermodynamic analysis of filling compressed gaseous hydrogen storage tanks," *International journal of hydrogen energy*, vol. 37, no. 6, pp. 5063-5071, 2012.

[3] M. C. Galassi, D. Baraldi, B. A. Iborra, and P. Moretto, "CFD analysis of fast filling scenarios for 70 MPa hydrogen type IV tanks," *International Journal of Hydrogen Energy*, vol. 37, no. 8, pp. 6886-6892, 2012.

[4] M. Striednig, S. Brandstätter, M. Sartory, and M. Klell, "Thermodynamic real gas analysis of a tank filling process," *International journal of hydrogen energy*, vol. 39, no. 16, pp. 8495-8509, 2014.

[5] TWI Ltd. "DEFECTS - HYDROGEN CRACKS IN STEELS - IDENTIFICATION." https://www.twi-global.com/technical-knowledge/job-knowledge/defects-hydrogen-cracks-in-steels-identification-045 (accessed.

[6] Hydrogen Fuel Cells, Engines, "Related Technologies–Module 1: Hydrogen Properties," *College of Desert*, 2001.

[7] "High Pressure Conforming Tank Technology." http://ioaircraft.com/innovation/conformingtanks.php (accessed.

[8] M. Li *et al.*, "Review on the research of hydrogen storage system fast refueling in fuel cell vehicle," *International Journal of Hydrogen Energy*, 2019.

[9] Engineering ToolBox. "Convective Heat Transfer." https://www.engineeringtoolbox.com/convective-heat-transfer-d_430.html (accessed.

[10] L. Gong *et al.*, "Spontaneous ignition of high-pressure hydrogen during its sudden release into hydrogen/air mixtures," *International Journal of Hydrogen Energy*, vol. 43, no. 52, pp. 23558-23567, 2018.

[11] J. Weisend. "Joule-Thomson Effect." https://cryogenicsociety.org/resources/defining_cryogenics/joule-thomson_effect/ (accessed.

[12] Wikipedia. "Joule–Thomson effect." https://en.wikipedia.org/wiki/Joule%E2%80%93Thomson_effect (accessed.

[13] H. K. Versteeg and W. Malalasekera, *An introduction to computational fluid dynamics: the finite volume method*. Pearson education, 2007.

[14] CFD-Online. "K-epsilon models." https://www.cfd-online.com/Wiki/K-epsilon_models (accessed.

[15] S. Wasserman. "Choosing the Right Turbulence Model for Your CFD Simulation." https://www.engineering.com/DesignSoftware/DesignSoftwareArticles/ArticleID/13743/Choosing-the-Right-Turbulence-Model-for-Your-CFD-Simulation.aspx (accessed.

[16] Wikipedia. "Law of the wall." https://en.wikipedia.org/wiki/Law_of_the_wall (accessed.

[17] Wolf Dynamics, "Finite Volume Method: A Crash introduction." [Online]. Available: http://www.wolfdynamics.com/wiki/fvm_crash_intro.pdf

[18] C. J. Greenshields, "OpenFOAM user guide," *OpenFOAM Foundation Ltd, version,* vol. 3, no. 1, p. e2888, 2015.

[19] OpenFoam. "rhoCentralFoam." https://www.openfoam.com/documentation/guides/latest/doc/guide-applications-solvers-compressible-rhoCentralFoam.html (accessed.

[20] C. J. Greenshields, "OpenFoam user guide. Version 6," *OpenFOAM Foundation Ltd July,* 2017.

[21] Pacific Northwest National Laboratory. "Hydrogen Compressibility at different temperatures and pressures." https://h2tools.org/hyarc/hydrogen-data/hydrogen-compressibility-different-temperatures-and-pressures (accessed.

[22] K. Johnson *et al.*, "Advancements and opportunities for on-board 700 bar compressed hydrogen tanks in the progression towards the commercialization of fuel cell vehicles," *SAE International Journal of Alternative Powertrains,* vol. 6, no. 2, 2017.

[23] X. Du, "Molecular-Dynamics Simulation of self-diffusion of molecular hydrogen in x-type zeolite," *Journal of Chemistry*, vol. 2013, 2013.

[24] University of California. "NASA polynomials." http://combustion.berkeley.edu/gri-mech/data/nasa_plnm.html (accessed.

[25] C. Greenshields. "Thermophysical models." https://cfd.direct/openfoam/user-guide/v6-thermophysical/ (accessed.

[26] CFD-Online, "Sutherland's law," 2008. [Online]. Available: https://www.cfd-online.com/Wiki/Sutherland's_law.

[27] Z. Tan, *Air pollution and greenhouse gases: from basic concepts to engineering applications for air emission control*. Springer, 2014.

[28] Yutopian. "Thermal Properties of Hydrogen." http://www.yutopian.com/Yuan/prop/H2.html (accessed.

[29] Pacific Northwest National Laboratory. "Hydrogen Density at different temperatures and pressures." https://h2tools.org/hyarc/hydrogen-data/hydrogen-density-different-temperatures-and-pressures (accessed.

[30] Pacific Northwest National Laboratory. "Hydrogen Viscosity at different temperatures and pressures." https://h2tools.org/hyarc/hydrogen-data/hydrogen-viscosity-different-temperatures-and-pressures (accessed.

Appendices

Appendix A: Density of Hydrogen [kg/m^3] in different pressure and temperature [29]

Temperature [°C]	Pressure [MPa]						
	0.1	**1**	**5**	**10**	**30**	**50**	**100**
-255	73.284	74.252					
-250	1.1212	68.747	73.672				
-225	0.5081	5.5430	36.621	54.812	75.287		
-200	0.5081	3.3817	17.662	33.380	62.118	74.261	
-175	0.3321	2.4760	12.298	23.483	51.204	65.036	
-150	0.2471	1.9617	9.5952	18.355	43.079	57.343	
-125	0.1968	1.6271	7.9181	15.179	37.109	51.090	71.606
-100	0.1636	1.3911	6.7608	12.992	32.614	46.013	66.660
-75	0.1399	1.2154	5.9085	11.382	29.124	41.848	62.322
-50	0.1223	1.0793	5.2521	10.141	26.336	38.384	58.503
-25	0.1086	0.9708	4.7297	9.1526	24.055	35.464	55.123
0	0.0976	0.8822	4.3036	8.3447	22.151	32.968	52.115
25	0.0887	0.8085	3.9490	7.6711	20.537	30.811	49.424
50	0.0813	0.7461	3.6490	7.1003	19.149	28.928	47.001
75	0.0750	0.6928	3.3918	6.6100	17.943	27.268	44.810
100	0.0696	0.6465	3.1688	6.1840	16.883	25.793	42.819
125	0.0649	0.6061	2.9736	5.8104	15.944	24.474	41.001

Appendix B: Dynamic viscosity [μPa.s] [30]

Temperature [°C]	Pressure [MPa]						
	0.1	**1**	**5**	**10**	**30**	**50**	**100**
-150	4.8497	4.9024					
-125	5.5131	5.5568					
-100	6.1394	6.1766	6.3447				
-75	6.7366	6.7691	6.9143	7.1114	8.1266		
-50	7.3098	7.3386	7.4668	7.6363	8.5079	9.4607	
-25	7.8624	7.8883	8.0031	8.1523	8.9119	9.7489	12.209
0	8.3969	8.4205	8.5245	8.6581	9.3275	10.077	12.241
25	8.9153	8.9369	9.0321	9.1533	9.7491	10.430	12.357
50	9.4193	9.4393	9.5270	9.6380	10.173	10.797	12.532
75	9.9102	9.9287	10.010	10.113	10.597	11.172	12.750
100	10.389	10.407	10.483	10.578	11.020	11.553	12.999
125	10.858	10.874	10.945	11.034	11.440	11.935	13.271

Appendix C: Assigned task description

University of South-Eastern Norway

Faculty of Technology, Natural Sciences and Maritime Sciences, Campus Porsgrunn

FMH606 Master's Thesis

Title: Simulation of hydrogen tank refuelling

USN supervisor: Knut Vågsæther

External partner: H2Maritime, Umoe Advanced Composites

Task background:
Hydrogen is a possible carbon free energy carrier as fuel for transportation, however there is a need for research and development of technology for handling and producing larger amounts of hydrogen for heavy duty transportation. For instance, in maritime applications larger amounts of hydrogen needs to be transported and refuelled during bunkering.

For maritime applications, the hydrogen storage tanks will be quite large and the filling rates will be high. The temperature field inside the tank will not be homogenous du to local stagnation of the gas. There is a maximum allowed local temperature on the walls of 85°C that needs to be upheld during refilling. To analyse different refuelling strategies and nozzle positions inside a large hydrogen tank, CFD-simulations need to be done. There is also a need for a simplified description of the thermodynamic states inside the tank.

This project is part of a larger research project on use of hydrogen for maritime transport (H2Maritime). More information on this project can be found here: https://ife.no/wp-content/uploads/2019/04/2019-04-26-Hydrogen-i-Transport-%C3%98ystein-Ulleberg-IFE.pdf

Task description:
- Literature study of tank refilling of gases
- CFD simulations of tank refilling for various filling procedures, boundary temperatures, nozzle positions etc.
- If time, make a simplified model (0D or 1D) based on CFD simulations where the variations of state is included

Student category: Must have had the CFD course

Practical arrangements: -

Supervision:
As a general rule, the student is entitled to 15-20 hours of supervision. This includes necessary time for the supervisor to prepare for supervision meetings (reading material to be discussed, etc).

Signatures:
Supervisor (date and signature): 11/5-2020 Knut Vågsæther

Student (write clearly in all capitalized letters): MASIH MOJARRAD

Student (date and signature): May 9th, 2020 Ma